34th Annual International Conference of the IEEE EMBS
San Diego, California USA, 28 August - 1 September, 2012

Numerical Simulations of Flow through the Aorta Using both Ideal and Realistic Geometrical Models

W. N. Wan Ab Naim, P. Ganesan, A. Al Abed, E. Lim

Abstract—**The effects of curvature and tapering on the flow progression in the aorta were studied using numerical simulations on a realistic geometrical model of the aorta and three different versions of the ideal aorta models. The results showed that tapering increases velocity magnitude and wall shear stress while local curvatures affect the skewness of the velocity profile, the thickness of the boundary layer as well as the recirculation regions. Wall shear stress distribution in the aorta serves as an important determinant in the progression of arterial disease**.

I. Introduction

Atherosclerosis refers to a condition in which the vessel wall thickens due to progressive build-up of plaque. The atherosclerosis normally localize in the part of curvature and branching in the arteries [1], such as the aortic arch, its major branches, and the abdominal aorta. Numerous studies have shown that the complicated geometry of the aorta, which involves more than one curvature planes, branching and distal tapering has a significant influence on the flow development, including the skewness of the axial velocity profile, recirculation, boundary layer growth and secondary velocities [2-3].The variations in the flow profiles lead to alterations in the wall shear stress distribution. In one study, Ku et al. [4] reported that low and fluctuating wall shear stress can be one of the factors in the development of atherosclerotic plaques, while higher wall shear stress has been linked with the formation and progression of aortic dissection [5]**.** On the other hand, Morris et al. [6] reported that recirculation promote the deposition of blood particles along the wall**.**

Since geometrical irregularities of the aorta and pulsatile nature of the aortic flow are believed to play an important role in the development of vascular disease, various studies have been performed on curved vessels to establish the relationship between the vessel curvature, Womersley number, and branching on the flow patterns [6-7]. In addition, in vitro experiments using rapid prototyping technique [3, 5], as well as computational fluid dynamics (CFD) study using either realistic geometry reconstructed from patients' images [6-7] or idealized geometry which mimics the geometry of the human aorta[8] have been extensively carried out. Morris *et al.* [6] showed that different image reconstruction techniques results in variations in the velocity profiles along the aortic arch, boundary layer thickness and recirculation regions. In another study, Wen *et al.* [5] investigated the pulsatile flow pattern and wall shear stress of a patient-specific thoracic aorta, taking into account the effect of the three branches on the aortic arch.

Due to the difficulty in obtaining accurate realistic geometries for the aorta, simple 3D geometrical representations are often used in CFD simulations, e.g. using constant cross-sectional areas along the aorta, removal of branches and removal of the out-of-plane curvature effects [3]. Although numerous studies have been carried out on either patient-specific geometries or ideal geometries, not many studies have specifically looked at relating the results from the ideal 3D geometrical models with that obtained from simulations using the realistic aorta geometries. In the present study, we exclude the three major branching arteries and focus on the effect of local curvature and tapering on the flow progression in the aorta at 2 different phases during the pulsatile flow, i.e. at maximum velocity and maximum deceleration. Four different model geometries were presented: (i) realistic 3D aorta reconstructed from the segmented CT images; (ii) ideal geometry with constant diameter along the aorta; (iii) ideal geometry with tapering effect; and (iv) ideal geometry with tapering effect and local curvature at the aorta entrance and descending aorta.

II. Methods

A. Model Geometry and Meshing

Four different model geometries as shown in Fig. 1(a)-(d) were studied, with their respective parameter values listed in Table 1. The normal aorta images taken from healthy subject (obtained from CT) were segmented, reconstructed and meshed with 4 nodes tetrahedral elements in ScanIP (Simpleware Ltd.). The diameter of the aorta for this subject as well as the amount of tapering (50%) from the ascending aorta to the beginning of the descending aorta falls within a reasonable range for a normal aorta [2, 9]. The three branches at the top of the aortic arch were removed as the focus of the present study is on the effect of curvature and tapering. On the other hand, the ideal geometries (constant diameter, tapering and curved) were drawn using SolidWorks 2008 (SolidWorks Corp.), with their parameters taken to represent normal aorta [8, 10]. Tetrahedral elements were assigned to each of the ideal geometry using Meshing in ANSYS CFD (ANSYS, Inc.).

*Research supported by University Malaya Research Grant.

W.N. Wan Ab Naim, P. Ganesan, E. Lim are with Department of Biomedical Engineering, Faculty of Engineering, University of Malaya, Kuala Lumpur 50603, Malaysia. (phone: 603-7967 6871; fax: 603-7967 7661; e-mail: einly_lim@um.edu.my).

A. Al Abed is with the Graduate School of Biomedical Engineering, the University of New South Wales, Sydney, 2052, Australia.

B. Model Properties and Boundary Conditions

The blood was assumed to be homogenous, incompressible and Newtonian with a dynamic viscosity of 0.00371 Pa.s and a density of 1060 kg/m^3. Even though blood tends to have non-Newtonian behavior at shear rate less than 100 s^{-1}, it has been observed that shear rate in large arteries is greater than 100 s^{-1} [5,11]. The aortic wall is assumed to be rigid. No-slip condition is applied at the wall [11]. The flow was assumed to be laminar. A flat, pulsatile velocity profile, as shown in Fig. 2a was applied at the entrance of the ascending aorta (adapted from Tse et al. [11]). On the other hand, a pulsatile pressure waveform as shown in Fig 2 (adapted from Tse et al. [11]) was applied at the exit of the descending aorta. The statement of the flat velocity profile specified at the aortic inlet is justified by in vivo measurements using the hot film anemometry technique on various animal models [5, 7].

The finite volume method in the ANSYS FLUENT package (ANSYS, Inc.) was used to run the simulations. Discretisation of the Navier-Stokes equation (equation (1) and (2) adapted from Wen et al. [5]) was achieved using the Second Order Upwind Scheme. The PISO (Pressure Implicit with Splitting of Operators) algorithm was used for the coupling of the pressure-velocity terms.

$$\nabla . \vec{v} = 0, \qquad (1)$$

$$\frac{\partial}{\partial t}(\rho \vec{v}) + \rho(\vec{v}.\nabla)\vec{v} = -\nabla p + \rho\vec{g} + \mu\nabla^2\vec{v} \qquad (2)$$

The symbol $\vec{v}$ is the velocity vector, p is the pressure, ρ is the density and μ is the viscosity.

A steady state solution at the maximum flow rate was first obtained. The solution was then used as the initial condition for the unsteady equation. In order to have the periodic nature of the flow, 4 cardiac cycles were run. The solution was obtained based on the results from the 5th cardiac cycle. During post processing, the geometries were divided into four regions of interest, i.e. the aortic arch entrance (section 1), mid-way along the aortic arch (section 2), aortic arch exit (section 3) and mid-way along the descending aorta (section 4), as shown in Fig. 3. Since the length of the vessels contributes to variations in the development of the boundary layer, the results for all the cases were taken at the same plane.

TABLE I. GEOMETRICAL PARAMETERS OF THE MODEL (D1 REPRESENTS THE DIAMETER AT THE ENTRANCE OF ASCENDING AORTA; D2 REPRESENT THE DIAMETER AT THE ENTRANCE TO DESCENDING AORTA; D3 REPRESENTS THE DIAMETER AT EXIT OF DESCENDING AORTA; Θ_1 REPRESENTS THE ANGLE AT THE DESCENDING PART AND Θ_2 REPRESENTS THE ANGLE AT ASCENDING PART OF AORTA.

Geometry	D1 (mm)	D2 (mm)	D3 (mm)	Θ_1, Θ_2
Ideal geometry (constant diameter)	22.5	22.5	22.5	0.0
Ideal geometry (tapering)	22.5	22.5	18.9	0.0
Ideal geometry (curved)	22.5	22.5	18.9	10.0, 6.0
Normal aorta	41.5	22.7	21.1	12.5,6.5

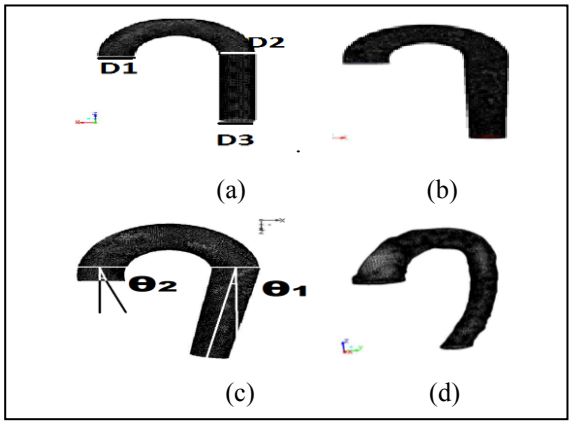

Figure 1. Four different geometrical representations of the aorta used in the present study: (a) ideal geometry (constnat diameter); (b) ideal geometry (tapering); (c) ideal geometry (curved); and (d) realistic aorta.

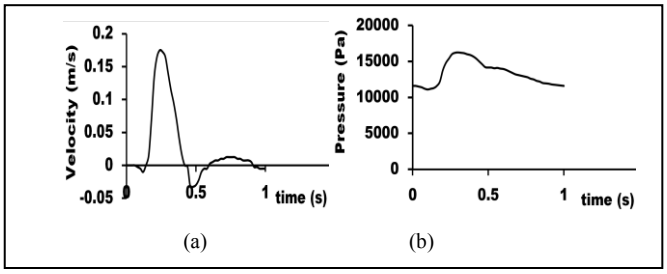

Figure 2. Inlet and outlet boundary conditions (adapted from Tse et al. [11]): (a) Pulsatile inlet velocity profile; and (b) Pulsatile outlet pressure profile.

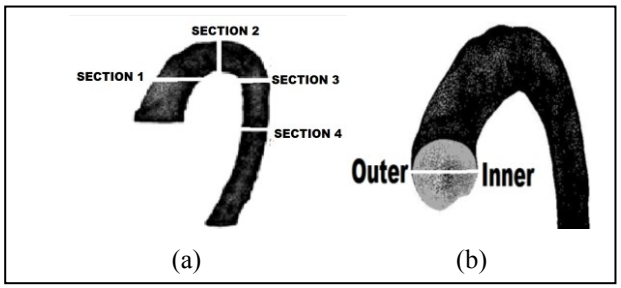

Figure 3. a) Four different regions along the aorta for the analysis of results: (i) the aortic arch entrance (section 1); (ii) mid way along the aortic arch (section 2); (iii) aortic arch exit (section 3); and (iv) mid way along the descending aorta (section 4); b) Figure represents the inner wall and outer wall of the curvature

III. RESULTS

A. Velocity Profiles

The results were taken at the four different regions along the aorta shown in Fig. 3, during maximum velocity (peak systole) and maximum deceleration (late systole).

Section 1: Aortic arch entrance: The flow begins as a flat profile at the entrance of the ascending aorta and travels up to the aortic arch entrance. At maximum flow velocity, the velocity profile for the ideal geometries (constant diameter and tapering) remains relatively flat (Fig. 4a). On the contrary, the local curvature effect at the ascending aorta for both the realistic geometry and the ideal geometry (curved) causes the velocity profile to skew towards the inner wall. The skewness in the velocity profile toward the inner wall at the aortic arch entrance agreed with that reported in the published literature [2-3, 6], and is believed to be caused by an imbalance between the centrifugal force and the radially inward pressure gradient in a curved tube, which draws fluid particles from the outer to the inner wall [12].

At maximum deceleration, boundary layer growth at both the inner and outer walls (more at the inner wall) can be observed for all geometries (Fig. 4b), due to a decrease in flow rate. Slight recirculation occurred at the inner wall for the ideal geometry (constant diameter and tapering) cases, which have thicker boundary layers as compared to the other two cases.

Sections 2: Aortic arch mid plane: As the flow travelled half way along the aortic arch, it is shown that the axial flow velocity profile in all geometries skewed toward the inner wall of the curvature (Fig. 5a), due to the curvature in the aortic arch, as has been reported by various studies [2-3, 6]. Higher mean velocities occur in the case of the realistic geometry as well as the ideal geometry (tapering) due to a decrease in the vessel diameter, particularly for the realistic geometry, which has a reduction of 50% in the diameter.

During maximum deceleration, the boundary layer at both the inner and outer walls in all geometries thickens, as compared to that at the aortic arch entrance (Fig. 5b), as reported by [6]. As a result, obvious recirculation vortex can now be seen near both the inner and outer walls of the realistic geometry, creating a v-shaped axial velocity profile.

Section 3: Aortic arch exit: Due to the growing boundary layer along the inner wall, the axial velocity profile is now shifting toward the outer wall for all geometries (Fig. 6a). During maximum deceleration, M-shaped axial velocity profile was observed for the realistic geometry, due to the slower moving velocity at the middle of the vessel, as also reported by [13] who uses realistic geometry in their simulations. However, this is not shown in the ideal geometry cases (only slightly in the tapering case) in our simulations, possibly due to the much lower velocity in these cases.

Section 4: Descending aorta: At the descending aorta, the axial velocity profiles for both the ideal geometry cases (constant diameter and tapering) flatten out at both maximum velocity and maximum deceleration (Fig. 7a). On the contrary, the velocity profiles for the realistic geometry and ideal geometry (curved) cases are skewed toward the outer wall at maximum velocity due to the curvature effect (curved inward) which induces strong centrifugal force. As suggested by [14], curvature plays a crucial role in shaping the profiles in the descending aorta. No recirculation is observed in all cases during maximum deceleration.

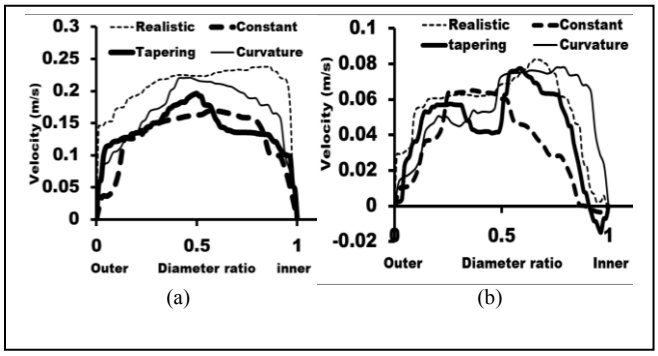

Figure 4. Velocity profiles at aortic arch entrance; a) Maximum velocity; b) Maximum deceleration

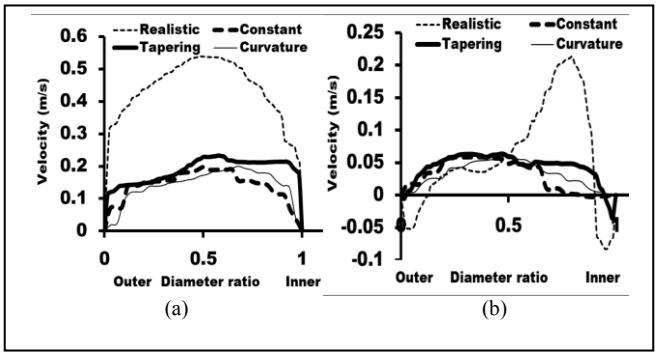

Figure 5. Velocity profiles at aortic arch mid plane; a) Maximum velocity; b) Maximum deceleration

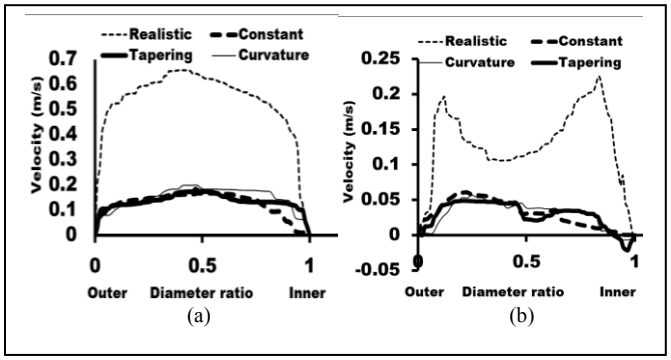

Figure 6. Velocity profiles at aortic arch exit; a) Maximum velocity; b) Maximum deceleration.

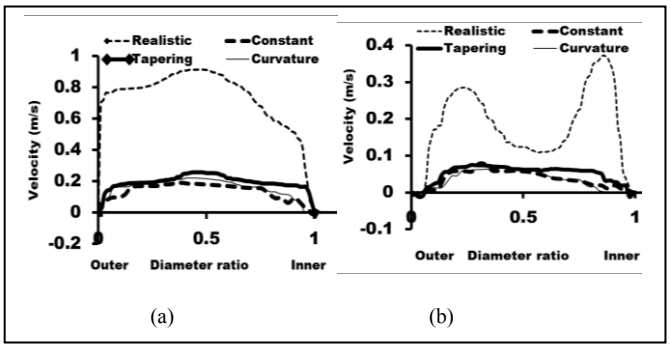

Figure 7. Velocity profiles at aortic arch exit; a) Maximum velocity; b) Maximum deceleration

B. *Wall Shear Stress*

The distribution of the wall shear stress along the aorta is largely dependent on the axial velocity gradient near the wall. At maximum velocity, except for the ideal geometry (constant diameter), we observed a higher wall shear stress at the descending aorta for the other cases due to a reduction in the diameter which results in an increase in the velocity magnitude (Fig. 8). Similar patterns were observed during maximum deceleration, but with an overall decrease in the wall shear stress magnitude caused by a decrease in the velocity. On the other hand, the wall shear stress was higher at the inner curvature part of the aortic arch for all geometries, as proven by [6]. This is caused by the skewing of the axial velocity profile toward the inner curvature of the aortic arch, which then results in an increase in the velocity gradient at that region. As the flow progresses to the descending aorta, the wall shear stress was higher near the outer wall in the realistic geometry and ideal geometry (tapering case) due to the skewness of the axial velocity profile toward the outer wall. Similar findings have been observed both experimentally and through numerical simulations [6]. If the ideal geometry is to be modified to simulate various diseases, such as aneurysm, regions of high and low wall shear stress is expected to be comparable to that using a realistic geometry. However, slight variations in the spatial distributions of the wall shear stress may occur due to more complicated realistic geometry (including surface roughness).

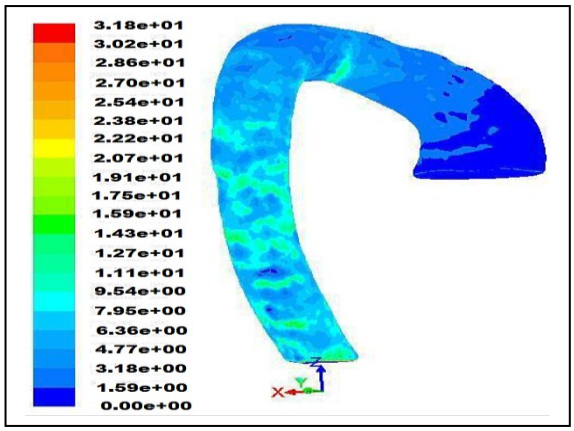

Figure 8. Wall shear stress distribution in the realistic aorta geometry at maximum velocity

IV. Conclusion

The present work investigates the effect of tapering and curvature on the axial velocity profile and wall shear stress distributions using ideal geometries and compares the results to that using the realistic aorta geometry. Results showed that tapering increases velocity magnitude and wall shear stress while local curvatures affect the skewness of the velocity profile, the boundary layer thickness as well as the recirculation regions. Wall shear stress, which has been shown to be an important determinant in the formation and progression of arterial diseases, is highly dependent on the axial velocity profile.

Acknowledgment

This study was funded by University Malaya Research Grant (RG109/11AET).

References

[1] Debakey, M.E., Lawries, G.M., Glaeser D.H., *Patterns of atherosclerosis and their surgical significance.* Annals of Surgery, 1985. **201**(12): p. 115-131.

[2] Chandran, K.B., *Flow dynamics in the human aorta.* Journal of Biomechanical Engineering, 1993. **115**: p. 611-616.

[3] Yearwood, T.L., & Chandran, K.B., *Physiological pulsatile flow experiments in a model of the human aortic arch.* J Biomechanical, 1982. **15**.

[4] Ku, D.N., Giddens, D.P, Zarins, C.K., & Glagov, S. (*Pulsatile flow and atherosclerosis in the human carotid bifurcation. Positive correlation between plaque location and low oscillating shear stress.* Arterioscler Thromb Vasc Biol, 1985. **5**: p. 293-302.

[5] Wen, C.Y., Yang, A.S., Tseng, L.Y., & Chai, J.W., *Investigation of pulsatile flowfield in healthy thoracic aorta models.* Annals of Biomedical Engineering, 2010. **38**(2): p. 391-402.

[6] Morris, L., Delassus, p., Callanan, A., Walsh, M., Wallis, F., & etc, *3-D Numerical simulation of blood flow through models of the human aorta.* Journal of Biomechanical Engineering, 2005. **127**.

[7] Shahcheraghi, N., Dwyer, H.A., Cheer, A.Y., Barakat, A.I., & Rutaganira, T., *Unsteady and three dimensional simulation of blood flow in the human aortic arch.* Journal of Biomechanical Engineering, 2002. **124**: p. 378-387.

[8] Vasava, P., Jalali, P., Dabagh, M., & Kolari, P.J., *Finite element modelling of pulsatile blood flow in idealized model of human aortic arch: Study of hypotension and hypertension.* Computational and Mathematical Methods in Medicine, 2012.

[9] Wolak, A., Gransar, H., Louise, E.J.T, *Aortic Size Assessment by Noncontrast Cardiac Computed Tomography: Normal Limits by Age, Gender, and Body Surface Area.* J A C C : C A R D I O V A S C U L A R I M A G I N G, 2008. **1**(2).

[10] Guan, J.C., Chu, B., Zhang, Y., Zeng, Y., & Qiao, A., *Three-Dimensional compuational simulation of bypassed aortic dissection.* IEEE, 2010.

[11] Tse, K., M., Ciu, P., Lee, H.P., & Ho, P., *Investigation of hemodynamics in the development of dissecting aneurysm within patient-specific dissecting aneurismal aortas using computational fluid dynamics(CFD) simulationss.* Journal of Biomechanics, 2011. **44**(827-836).

[12] Chandran, K.B., *Flow dynamics in the human aorta.* 2001.

[13] Seed, W.A.W., N.B., *Velocity patterns in the aorta.* Cardiovascular Research, 1971. **5**: p. 319-330.

[14] Falsetti, H.L., Kiser,K.M., Francis,G.P., & Belomore, E.R., *Sequential velocity development in the ascending and descending aorta of the dog.* Journal of the American Heart Association, 1972. **31**: p. 328-338.